M. A. Hamilton

M. C. Sucec

B. J. Fregly

Department of Mechanical and Aerospace Engineering,
University of Florida,
Gainesville, FL 32611

S. A. Banks

Department of Mechanical and Aerospace Engineering,
University of Florida,
Gainesville, FL 32611
and Orthopaedic Research Lab,
The Biomotion Foundation,
Palm Beach, FL 33480

W. G. Sawyer[1]

e-mail: wgsawyer@ufl.edu
Department of Mechanical and Aerospace Engineering,
University of Florida,
Gainesville, FL 32611
e-mail: wgsawyer@ufl.edu

Quantifying Multidirectional Sliding Motions in Total Knee Replacements

This manuscript describes a formulaic method to predict the severity of crossing motions experienced by ultra-high-molecular-weight polyethylene (UHMWPE) under sliding conditions across a bearing surface. A statistical model for evaluating the distribution of sliding about this orientation is described. This model compares favorably to published experimental data on UHMWPE under multidirectional pin-on-disk testing. These algorithms are applied to the tibial component of a total knee replacement using patient-specific kinematics for gait and stair-rise activities collected using fluoroscopy. A dynamic contact model is used to calculate contact pressures and slip velocities on individual surface elements from this kinematic data. The most significant degree of crossing motion intensity was observed in the lateral compartments for both gait and stair-rise activities. This coincided with the location of maximum tribological intensity. The maximum crossing motions are characteristic of 4 and 9 deg of bidirectional crossing motion for gait and stair, respectively. [DOI: 10.1115/1.1843136]

Introduction

Debris particle generation of ultra-high-molecular-weight polyethylene (UHMWPE) remains a clinical issue in total joint replacements such as knees and hips. Significant advances in modeling and understanding the origin of wear debris liberation in total hip replacements have been made over the past decade. One recently discovered aspect is the importance of sliding direction on wear in UHMWPE. From the perspective of an individual material element on the UHMWPE surface, variations in sliding direction appear as transverse crossing motion in equivalent pin-on-disk experiments. Orders of magnitude changes in wear rate with increasing degrees of crossing motion have been reported [1–4].

In contrast to the hip, where axisymmetric conformal contact has facilitated wear-related studies [1,4–7], the knee produces complex motions that have prevented detailed study of tibial insert crossing patterns. Locus plots (Fig. 1), which seek to represent the kinematics by following the most probable trajectory of contact on the surface, do not capture the relative motions experienced by particular surface locations. To capture this information, it is necessary to determine both the pressure and slip velocity at individual surface locations at any instant in an activity cycle. While slip velocity vectors can be plotted for individual surface locations [4] (Fig. 2), they cannot be plotted for all locations simultaneously to visualize crossing on the entire surface. Thus, a new approach is needed to visualize the extent of crossing experienced by *all* locations on the surface *simultaneously* over an entire activity cycle.

This study presents a new statistical formulation for quantifying and visualizing the intensity of crossing motions experienced by all locations on the UHMWPE tibial insert surface simultaneously over any specified time duration. The formulation combines the calculation of tribological quantities with the estimation of the most probable direction of polymer orientation. The reasonableness of the formulation is evaluated using data from pin-on-disk experiments and the practical value demonstrated using computer simulation of a total knee replacement for which in vivo kinematic data and a post-mortem retrieved tibial insert were available. In addition, counterface motions are suggested for researchers screening new tribological materials using bidirectional pin-on-disk tribometers. The results provide valuable information to address the use of cross-linked UHMWPE in total knees.

Theoretical Development of Crossing Motion Analysis

The proposed analysis of crossing motion requires contact pressure and slip velocity time histories for individual elements on the worn surface. The analysis is based on sequential calculation of five quantities. The first is tribological intensity τ defined as

$$\tau = p|\mathbf{d}| \tag{1}$$

where $\mathbf{d}$ is the slip vector created by multiplying the instantaneous slip velocity by the simulation time increment and p is contact pressure. Equation (1) is related to Archard's wear law, which gives a depth of wear proportional to the product of the contact pressure and the sliding distance, and suggests that crossing is detrimental only if the element is in contact and experiencing relative motion.

The second quantity is dominant orientation of tribological intensity $\bar{\theta}$ defined as

$$\bar{\theta} = \sum_{i=1}^{n} \tau_i \theta_i \Big/ \sum_{i=1}^{n} \tau_i \tag{2}$$

where i indicates the current time during the activity and θ_i indicates the instantaneous crossing orientation relative to a fixed

[1]Corresponding author. Telephone: (352) 392-8488.

Contributed by the Tribology Division for publication in the ASME JOURNAL OF TRIBOLOGY. Manuscript received by the Tribology Division January 24, 2003 revised manuscript received March 10, 2004. Review conducted by: M. D. Bryant.

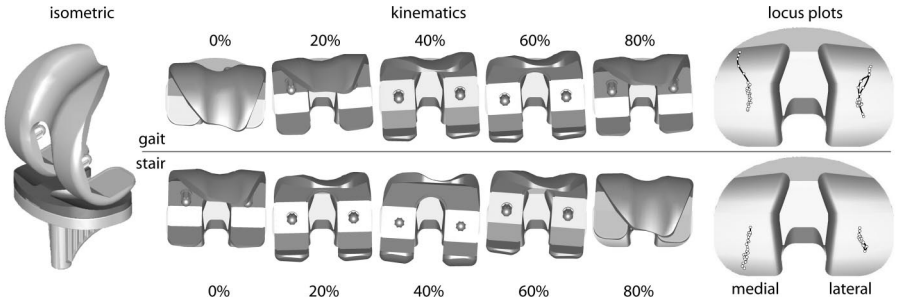

Fig. 1 Component design and film strips of the kinematics for the gait and stair rise activities. The corresponding locus plots of contact pressure centroid are shown to the far right. The five poses at different times through an activity cycle clearly show the rotations of the femoral component about the surface normal of the UHMWPE tibial bearing.

medial-lateral axis. θ_i is restricted to be between 0 and π since reciprocating motion is expected to produce a single primary orientation (in the article, 100 point discretized motions are used for all calculations). Equation (2) weights each θ_i by the corresponding τ_i and then normalizes to define the most probable direction of polymer orientation for a particular element after significant sliding (i.e., the tribological interface dominates over the earlier manufactured interface). This equation is motivated by the observation that unidirectional motions produce significantly less wear than do multidirectional motions in laboratory tests [3,4,8], hip joint simulator tests [1], and modeling studies [2,4].

The third quantity is crossing intensity σ defined as

$$\sigma = \sqrt{\sum_{i=1}^{n} (\tau_i \Delta\theta_i)^2 \Big/ n} \tag{3}$$

where $\Delta\theta_i = \bar{\theta} - \theta_i$. Equation (3) weights each τ_i value by how much its associated slip direction deviates from the dominant orientation direction. Unlike the extreme value parameter proposed in Ref. [4], this equation is motivated by rms error calculations that weight values more heavily the farther they are from zero while producing a single value to represent the entire motion. The presumed lowest-wear scenario, unidirectional motion in the direction of $\bar{\theta}$, would produce $\sigma = 0$ regardless of the τ_i values since no crossing would occur.

The fourth quantity is a worst-case crossing intensity σ_0 defined for normalization purposes. This quantity is needed to turn σ into a dimensionless quantity that can be easily interpreted for any given motion. The assumed worst-case situation is uniform circular counterface motion (i.e., $|\mathbf{d}| = \text{constant}$) with constant applied pressure (i.e., $p = \text{constant}$). From Eq. (1), this implies that τ_i is a constant whose value is unknown. However, to calculate σ_0 from Eq. (3), τ_i as well as $\Delta\theta_i$ must be known. For a circular counterface motion, $\Delta\theta_i$ varies uniformly with time and $\bar{\theta} = \pi/2$ (see Fig.

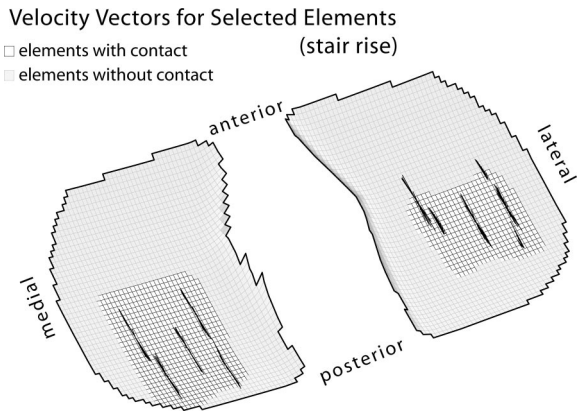

Fig. 2 Overlaying plots of velocity vectors, normalized by the largest velocity vector in the simulation, onto the corresponding elements on the tibial mesh. These vectors are from a stair-rise activity, which shows the greatest degree of crossing motion.

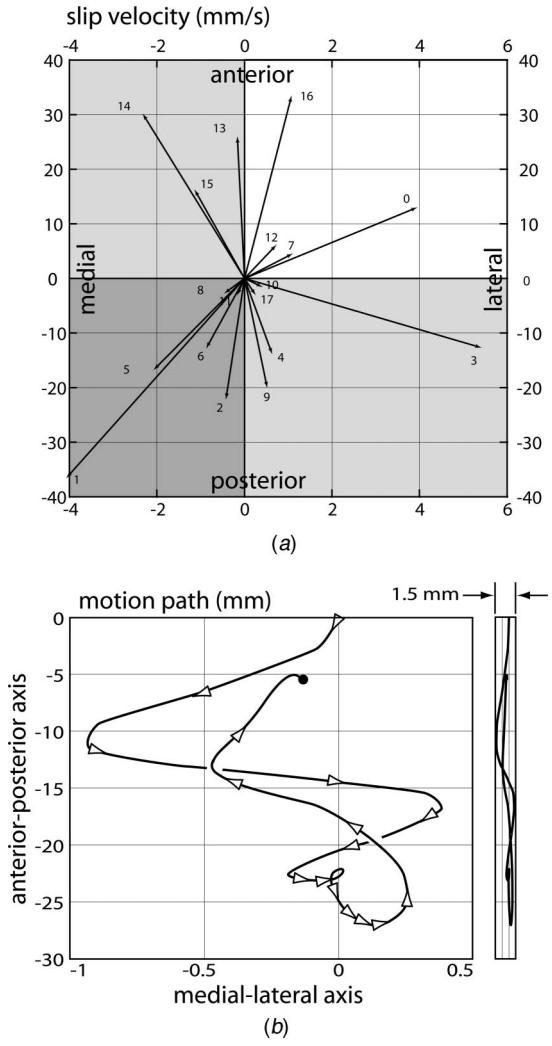

Fig. 3 (*a*) Vector plot of the counterface slip velocities at a particular location in the lateral compartment for 17 different instances during stair rise (vectors are numbered in chronological order). This location had a fairly typical motion profile. (*b*) The motion path of the femoral component over this location. Notice the medial-lateral axis is exaggerated by 20 times, with a 1-to-1 motion path shown to the right; the arrow heads are uniformly spaced in time.

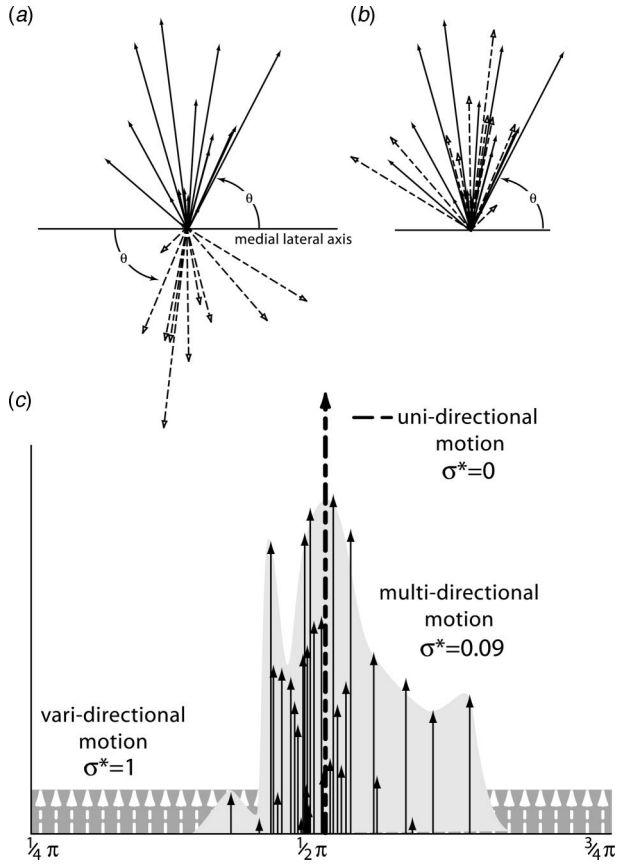

Fig. 4 (*a*) Vector plot for tribological intensities shown with the angular coordinate convention. (*b*) Overlaying plot with angular coordinate. (*c*) Scatter plot of tribological intensity versus angular coordinate compared with unidirectional motion (delta function) and multidirectional motion defined by the circular path (step function).

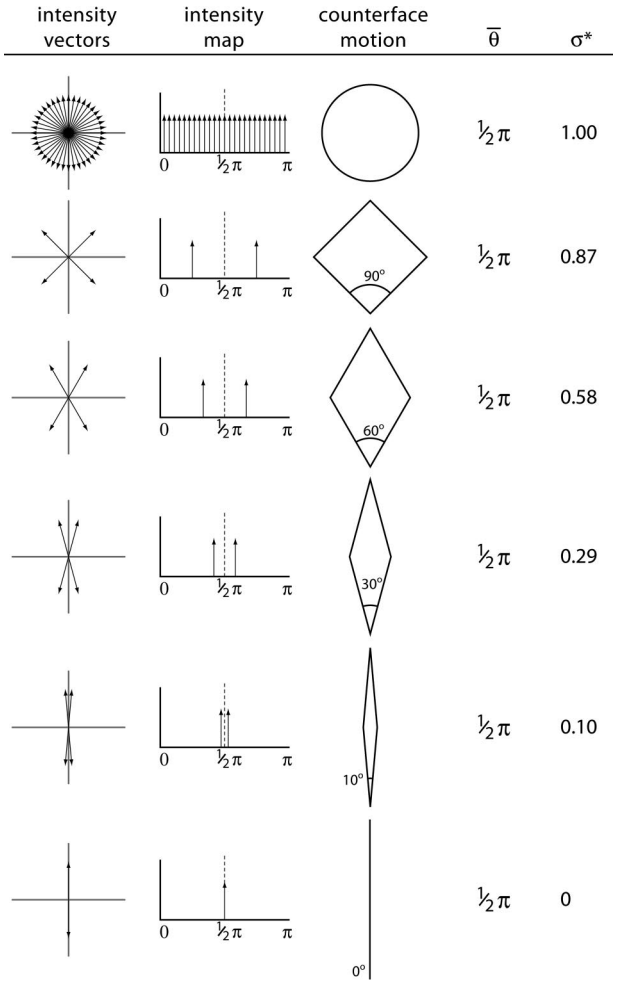

Fig. 5 A series of simple bidirectional intensity maps, with corresponding counterface motion and normalized crossing intensity σ^*

A1). A constant value of τ_i can be calculated by assuming the cumulative tribological intensity of the uniform circular motion equals the cumulative tribological intensity of the motion being analyzed.

The final quantity calculated is the normalized crossing intensity σ^* defined as

$$\sigma^* = \sigma/\sigma_0 \tag{4}$$

This quantity is used as a single dimensionless measure of crossing intensity. In this study, σ^* was calculated for every element on the medial and lateral tibial insert contact surfaces for both the gait and stair simulations. For computational efficiency, σ and σ_0 can be calculated simultaneously when solving for σ^*.

It is helpful to visualize the slip velocity vectors and corresponding motion path for a specific location on the tibial insert surface (Fig. 3). As can be seen from the locus plot (Fig. 1), this patient exhibited lateral pivoting during stair rise. The elements in the lateral compartment were in contact for the largest number of time steps; thus, they provided the most interesting vector-plots. In Fig. 3 the x axis, which is the medial-lateral axis, of the slip velocity plot is exaggerated by almost an order of magnitude. In the motion path plot, these slip velocities are multiplied by the time increment to give incremental displacements of the femoral component over the element. These incremental motion vectors are strung head to tail to give a motion path. In this plot the medial-lateral axis is exaggerated 20 times, while an unexaggerated motion path is shown on the right. The arrow heads on the motion path plot are evenly spaced by time, and some information about sliding speed at various locations along the path can be gleaned. Figure 4 shows the tribological intensity vector plots and scatter plots for this data.

Crossing motion can be easily conceptualized using a bidirectional diamond pattern, in which a square has a crossing angle of 90 deg. Figure 5 shows a series of simple counterface motions. The usefulness of normalized crossing intensity is immediately obvious; the circular motion gives $\sigma^*=1$, the reciprocating motion gives $\sigma^*=0$, and the narrowing diamond patterns span the range smoothly. These plots were created assuming a constant applied contact pressure.

Experimental Quantification on the Effect of Crossing Intensity on Wear

A study was conducted by Turrell et al. [8] to ''validate an earlier theory proposed by Wang [4] known as the unified theory of wear for UHMWPE in multidirectional sliding or orientation softening-wear model.'' This model offers a dependence of the wear rate k on the ratio of the perpendicular sliding distance A to the sum of the sliding distance in the principal direction of motion B and perpendicular direction A. This is given in Eq. (5) as

$$k \propto \frac{A}{A+B} \tag{5}$$

The experiments reported in Ref. [8] used GUR 1050 unsterilized UHMWPE pins loaded against implant grade cobalt chrome disks

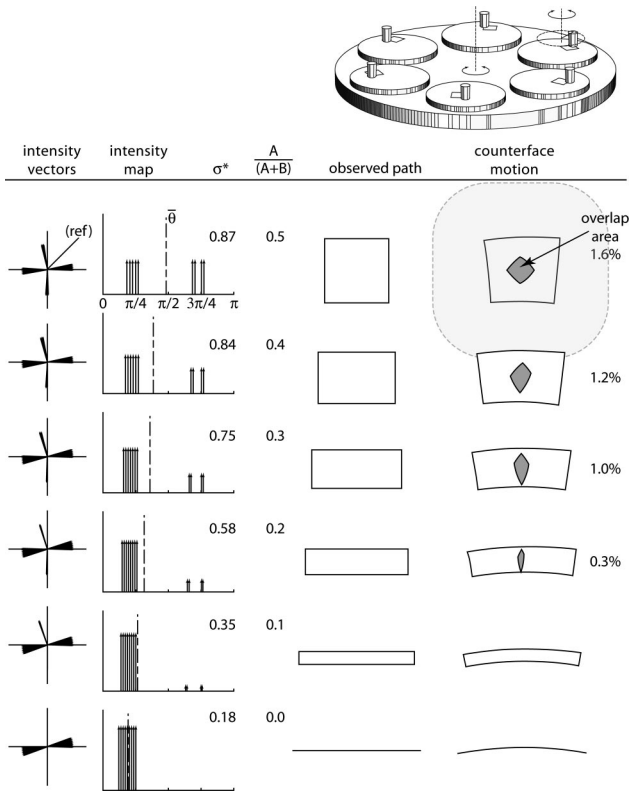

Fig. 6 A series of intensity maps, with corresponding counterface motion and normalized crossing severity index for the experiments conducted in Ref. [8]. The central point on the UHMWPE pin is analyzed. The observed path is on the counterface, and the curved paths are the equivalent paths for a nonrotating pin.

in diluted bovine serum on an OrthoPOD™ multidirectional tribometer. By commanding the rotations of an eccentrically mounted pin loaded against a rotary table, the OrthoPOD™ can prescribe various crossing motions between the counterface and UHMWPE pins. The rotational kinematics of the machine are illustrated in Fig. 6. Of great importance to these experimental data is that the rectangular paths are programmed onto the counterface samples using a point-to-point ''teach mode.'' These rectangular paths are created through two rotations (i.e., the rotation of the disk specimens and the rotation of the eccentrically mounted pins), and any straight line paths along the disk surface require the pin to rotate relative to the disk. The consequence of this on the sliding velocity vectors of the center point of the pin specimen relative to the disk specimen is clearly evident in Fig. 5, where plots of tribological intensity are not the twin delta functions separated by $\pi/2$ as the authors hoped, but rather a spread of velocities tightly packed about directions that are close to $\pi/2$ apart.

In Fig. 6, the normalized crossing intensity σ^* is calculated for the six different experiments that were performed and compared to the reported $A/(A+B)$ ratio. It is interesting to note the nonzero value of σ^* at the linear path on the counterface, and the significant amounts of overlap in the motion at the higher crossing motion experiments. In Fig. 7(*a*) the data from these experiments is plotted according the $A/(A+B)$ ratio, and in Fig. 7(*b*) the data are plotted according the normalized crossing intensity. The data shows a clear relationship to the square of normalized crossing intensity.

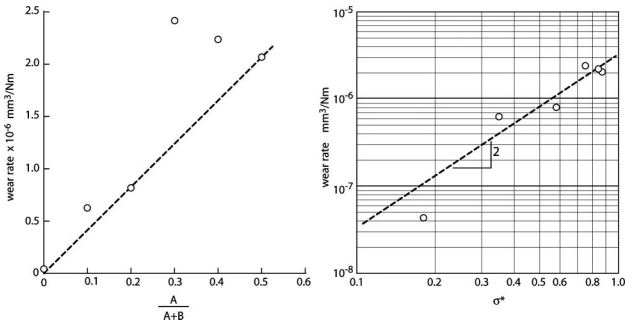

Fig. 7 Plots of the experimental data from Ref. [8] (*a*) versus the ratio of the secondary perpendicular motion to the total motion for a rectangular path, and (*b*) versus the normalized crossing intensity σ^* as calculated in Fig. 6

Computational Application to a Total Knee Replacement

To investigate the significance of crossing motions in total knee replacements, an analysis was performed on a knee implant for which in vivo fluoroscopic data as well as the post-mortem retrieved tibial insert were available. Fluoroscopic kinematic data were collected from one total knee arthroplasty patient: female, age 65 at time of surgery, height 170 cm, mass 70 kg [9]. The implanted component was a cemented posterior cruciate ligament

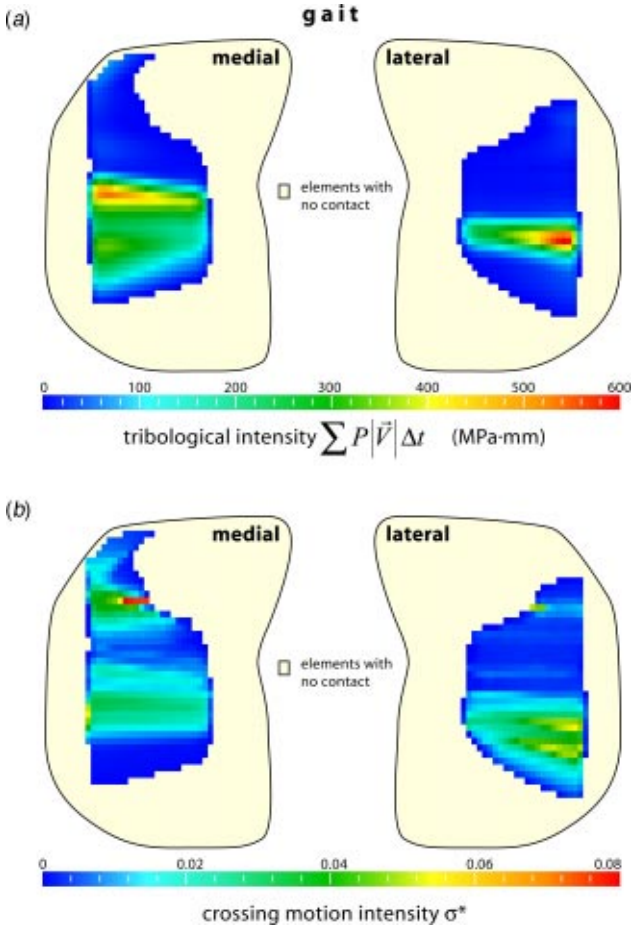

Fig. 8 Contour maps of (*a*) tribological intensity and (*b*) normalized crossing intensity σ^* defined for elements in contact during gait plotted over the projected areas of the tibial bearing compartments

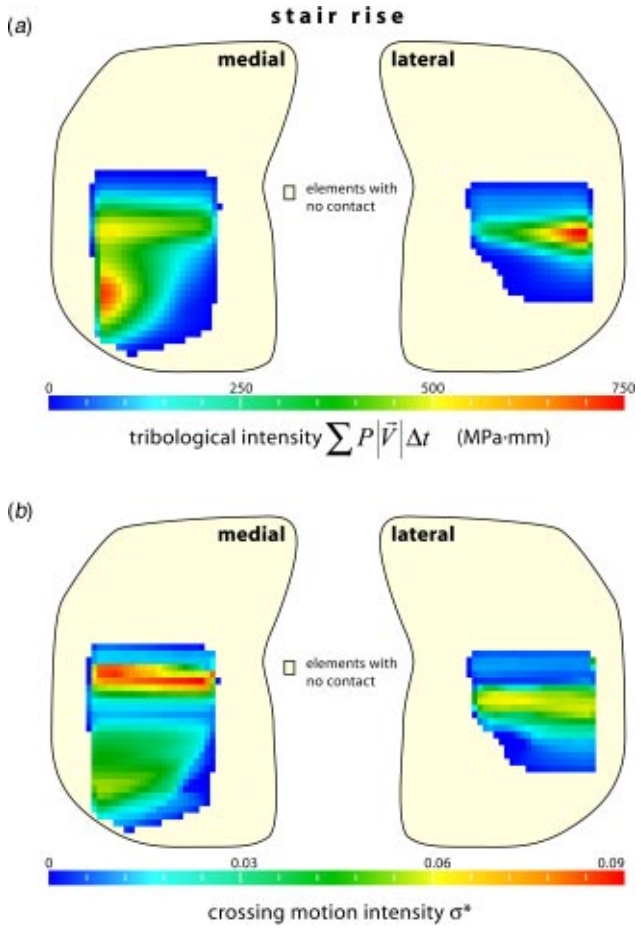

Fig. 9 Contour maps of (*a*) tribological intensity and (*b*) normalized crossing intensity σ^* for elements in contact during stair rise plotted over the projected areas of the tibial bearing compartments

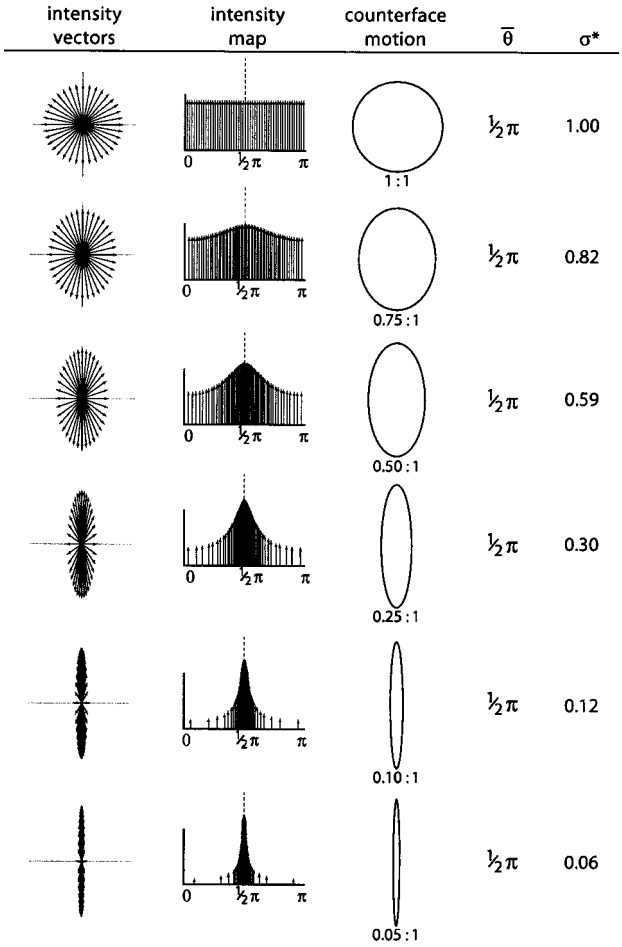

Fig. A1 A series of simple intensity maps for elliptical contacts of varying aspect ratio

retaining prosthesis (Series 7000, Stryker Howmedica Osteonics, Inc, Allendale, NJ) with a 6.8-mm-thick insert. The collected kinematics of this implant and patient are shown in Fig. 1, with a locus plot describing the path of the contact pressure centroid over the insert for the various activities.

The patient performed treadmill gait and stair rise/descent activities during fluoroscopic motion analysis [10–12] 21 months after surgery. Fluoroscopic analysis matches three-dimensional geometric constructions of the prosthetic components to the two-dimensional fluoroscopic images. The technique is accurate to approximately 1 deg for all rotations and 0.5 mm for translations in the sagittal plane [10]. Kinematic data from one representative cycle of each activity was averaged in 5 deg increments of knee flexion for stair and 1% increments for gait, including stance and swing phases.

A dynamic simulation of the patient's in vivo knee mechanics was created by incorporating an elastic contact model into a commercial multibody dynamics software program (Pro/MECHANICA MOTION, Parametric Technology Corporation, Waltham, MA). This approach was taken to predict joint kinematics and contact pressures in a fraction of the time possible with current dynamic finite-element methods [13–15]. The contact model uses elastic foundation theory [16–19] and treats the tibial insert as an elastic layer contacting a rigid femoral component. This model formulation accommodates the finite thickness and dimensions of the tibial insert, conformal or nonconformal contact situations, and linear or nonlinear polyethylene material properties [20]. The elastic contact model was implemented as a dynamic link library that can be incorporated into any multibody dynamics software.

The elastic foundation approach calculates contact pressures on a grid of elements covering the tibial insert contact surfaces. The elements define a ''bed of springs'' in which each spring is independent from its neighbors [16]. This approximation eliminates the integral nature of contact problems, thereby greatly simplifying the analysis of conformal geometry or nonlinear materials. For any element, given the interpenetration δ between the undeformed tibial and femoral surfaces in the direction of the local surface normal, the contact pressure p acting on the element can be calculated from [16–18]

$$p = \frac{(1-\nu)E}{(1+\nu)(1-2\nu)}\frac{\delta}{h} \tag{6}$$

where E is Young's modulus of the elastic layer, ν is Poisson's ratio of the elastic layer, and h is the layer thickness at that location. The interpenetration δ for each element is calculated using the ACIS 3D Toolkit (Spatial Corporation, Westminster, CO). The resulting element pressures are multiplied by their corresponding areas to produce a set of point forces. These forces are replaced with a single equivalent force and torque applied to both bodies for purposes of dynamic simulation [21].

Calculation of accurate slip velocities and contact pressures on individual surface elements requires the dimensions of the simulated contact patch to match in vivo conditions. The ability of the elastic foundation contact model to predict contact areas and pressures was evaluated experimentally using 16 different in vitro

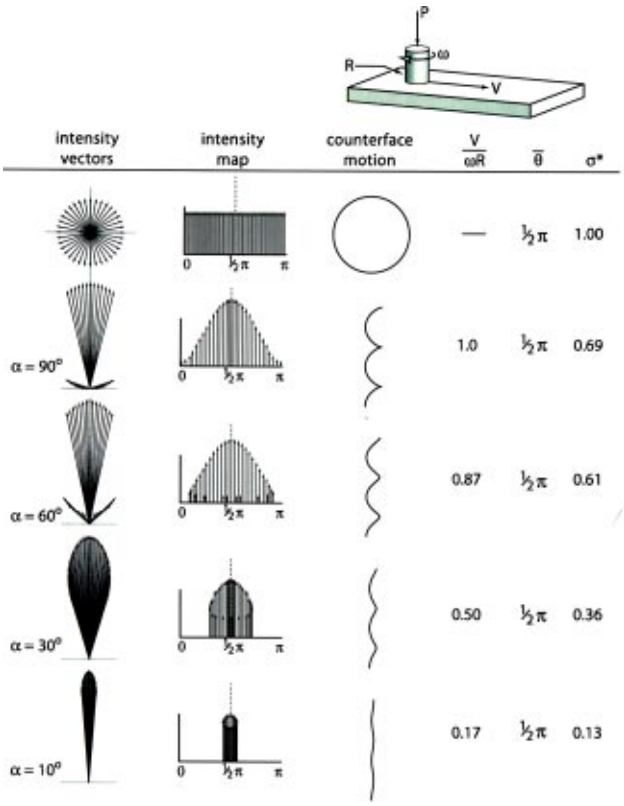

Fig. A2 A series of intensity maps with corresponding counterface motion and normalized crossing severity index for the combined rotating and translating pin geometry [4]. The nomenclature is α is an extreme value half-angle for the slip velocity vectors, *P* is contact pressure, ω is the angular velocity of the pin, *R* is the pin radius, and *V* is the translating speed of the pin. The pin is made of UHMWPE and is sliding on a flat polished counterface. The equivalent counterface motions are relative to a differential element on the edge of the pin.

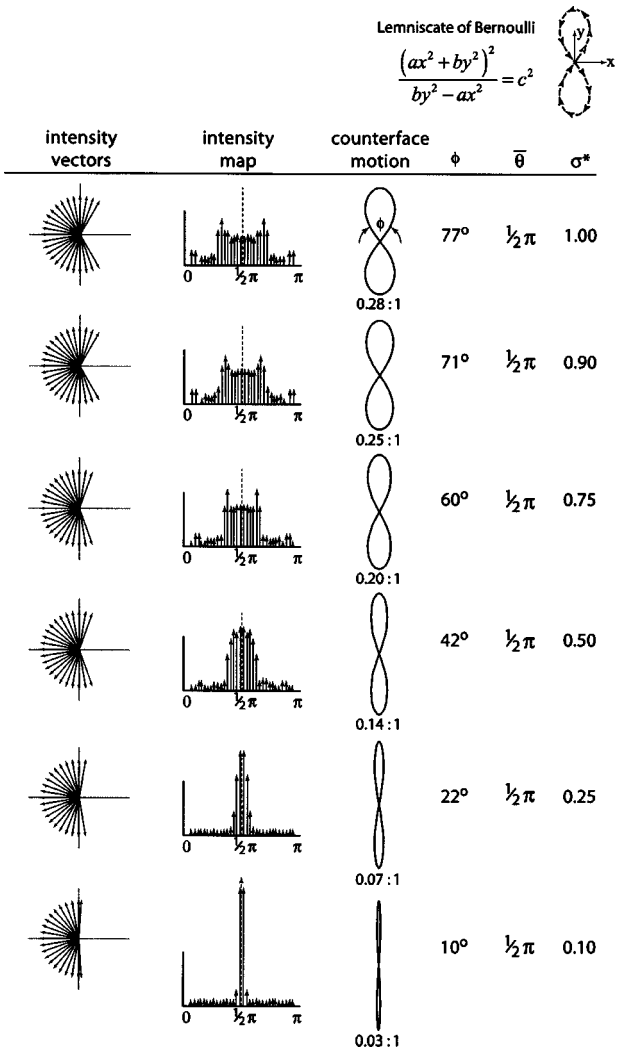

Fig. A3 A series of intensity maps with corresponding counterface motion and normalized crossing severity index for figure eight motion paths. In this model the pin is stationary and the counterface moves in the prescribed pattern beneath the pin.

static loading conditions (loads of 750, 1500, 2250, and 3000 N and flexion angles of 0, 30, 60, and 90 deg [20]). For each condition, experimental pressure measurements were made with a Tekscan K-Scan sensor. Using linear polyethylene material properties, the model was able to predict experimentally measured average contact pressures between 5 to 17 MPa with a mean error of 0.3 MPa and standard error of 0.5 MPa. Since contact forces were matched exactly on each side via static analysis, contact areas were also well predicted.

Dynamic simulations representing patient-specific in-vivo conditions were generated by combining in-vivo fluoroscopic measurements with assumed loading conditions. In the dynamic contact model, the femoral component possessed six degrees of freedom (DOFs) relative to the tibial insert. Three DOFs (anterior-posterior translation, internal-external rotation, and flexion) were prescribed to match fluoroscopically measured gait and stair kinematics (two separate simulations). The remaining three DOFs (axial translation, varus-valgus rotation, and medial-lateral translation) were numerically integrated to predict their motion (see [13] for further details). An axial force was applied vertically downward to the femoral component to produce a 70% medial–30% lateral load split at 0 deg flexion [22–24]. The axial force curve for each activity was defined by scaling a vertical ground reaction force curve [25–27] to be between 0.25 and 3.0 times body weight [23,25–27]. Ground reaction force data were taken from a patient of similar age, height, weight, and knee flexion characteristics.

The dynamic contact model generated contact pressures and slip velocities in two steps. First, a forward dynamics simulation calculated contact forces and kinematics. Then an inverse dynamics analysis used the results from the forward dynamics simulation to calculate contact pressures and slip velocities over a 50×50 element grid on each tibial contact surface. The predicted contact pressures and slip velocities for individual surface elements were used as inputs to the proposed analysis of crossing motion.

Computational Results and Discussion

The crossing motion analysis was applied to the patient kinematic data for two activities—gait and stair rise—and contour plots of tribological intensity and normalized crossing intensity σ^* were generated (Figs. 8 and 9). Both gait and stair activities showed limited normalized crossing intensity with maximum $\sigma^*\cong0.09$. The coincidence of highest crossing intensity with greatest tribological intensity occurs on the lateral compartments for both activities. This is believed to be due to the pivoting nature of this patient's kinematics. While the plots of crossing and tribological intensity are similar, location of maximum values are not necessarily coincident. The crossing motions observed for this pa-

tient are mathematically similar to that from uniform bidirectional patterns with 10 deg of included angle, which is a potentially useful screening motion for pin-on-disk testing.

Asymmetrically conforming knee prostheses are currently available, with designed lateral or medial pivoting. The challenges in evaluating the potential tribological impact of such designs require evaluation of both tribological intensity and crossing intensity.

Closure

Formulaic methods for calculating tribological intensity, probable orientation direction, and normalized crossing intensity are proposed. The approach compares favorably to existing data on UHMWPE under multidirectional tribology testing. These methods have been demonstrated and applied to a tibial component of a total knee replacement using the patient's in-vivo kinematics for gait and stair activities. Overall, the patient showed limited crossing motion with highest crossing intensities occurring on the lateral side. In the future, this methodology may be useful for analyzing new knee designs prior to clinical use to assess the likelihood of UHMWPE damage due to significant crossing motion.

Appendix

Intensity Maps for Various Multidirectional Motions. Many research groups are modeling the effects of multidirectional motion on wear of the UHMWPE, and simple motions are prescribed for these experiments using various multidirectional pin-on-disk tribometers. In this appendix, Figs. A1, A2, and A3 give similar plots for elliptical counterface motion, combined rotating and translating pins, and figure eights, respectively. These plots are done assuming a constant contact pressure.

References

[1] Bragdon, C. R., O'Conner, D. O., Lowenstein, J. D., Jasty, M., and Syniuta, W. D., 1996, ''The Importance of Multidirectional Motion on the Wear of Polyethylene,'' IMechE Part H: Journal of Engineering in Medicine, **210**, pp. 157–165.

[2] Muratoglu, O. K., Bragdon, C. R., O'Connor, D. O., Jasty, M., Harris, W. H., Gul, R., and McGarry, F., 1999, ''Unified Wear Model for Highly Crosslinked Ultra-High Molecular Weight Polyethylenes (Uhmwpe),'' Biomaterials, **20**, pp. 1463–1470.

[3] Burroughs, B. R., and Blanchet, T. A., 2001, ''Factors Affecting the Wear of Irradiated Uhmwpe,'' Tribol. Trans., **44**, pp. 215–223.

[4] Wang, A., 2001, ''A Unified Theory of Wear for Ultra-High Molecular Weight Polyethylene in Multi-Directional Sliding,'' Wear, **248**, pp. 38–47.

[5] Maxian, T. A., Brown, T. D., Pedersen, D. R., and Callaghan, J. J., 1996, ''3-Dimensional Sliding/Contact Computational Simulation of Total Hip Wear,'' Clin. Orthop. Relat. Res., pp. 41–50.

[6] Kurtz, S. M., Ochoa, J. A., Hovey, C. B., and White, C. V., 1999, ''Simulation of Initial Frontside and Backside Wear Rates in a Modular Acetabular Component With Multiple Screw Holes,'' J. Biomech., **32**, pp. 967–976.

[7] Meyer, D. M., and Tichy, J. A., 1999, ''Lubrication Model of an Artificial Hip Joint: Pressure Profile Versus Inclination Angle of the Acetabular Cup,'' ASME J. Tribol., **121**, pp. 492–498.

[8] Turrell, M., Wang, A., and Bellare, A., 2003, ''Quantification of the Effect of Cross-Path Motion on the Wear Rate of Ultra-High Molecular Weight Polyethylene,'' Wear, pp. 1034–1039.

[9] Harman, M. K., Banks, S. A., and Hodge, W. A., 2001, ''Polyethylene Damage and Knee Kinematics After Total Knee Arthroplasty,'' Clin. Orthop. Relat. Res., pp. 383–393.

[10] Banks, S. A., and Hodge, W. A., 1996, ''Accurate Measurement of Three-Dimensional Knee Replacement Kinematics Using Single-Plane Fluoroscopy,'' IEEE Trans. Biomed. Eng., **43**, pp. 638–649.

[11] Banks, S. A., Markovich, G. D., and Hodge, W. A., 1997, ''The Mechanics of Knee Replacements During Gait: In Vivo Fluoroscopic Analysis of Two Designs,'' Am. J. Knee Surgery , **10**, pp. 261–267.

[12] Banks, S. A., Markovich, G. D., and Hodge, W. A., 1997, ''In Vivo Kinematics of Cruciate-Retaining and Substituting Knee Arthroplasties,'' J. Arthroplasty, **12**, pp. 297–304.

[13] Fregly, B. J., Sawyer, W. G., Harman, M. K., and Banks, S. A., 2004, ''Computational Wear Prediction of a Total Knee Replacement From In Vivo Kinematics,'' J. Biomech., **38**, pp. 305–314.

[14] Giddings, V. L., Kurtz, S. M., and Edidin, A. A., 2001, ''Total Knee Replacement Polyethylene Stresses During Loading in a Knee Simulator,'' ASME J. Tribol., **123**, pp. 842–847.

[15] Godest, A. C., Beaugonin, M., Haug, E., Taylor, M., and Gregson, P. J., 2002, ''Simulation of a Knee Joint Replacement During a Gait Cycle Using Explicit Finite Element Analysis,'' J. Biomech., **35**, pp. 267–275.

[16] Johnson, K. L., 1985, *Contact Mechanics*, Cambridge University Press, Cambridge, UK.

[17] An, K. N., Himeno, S., Tsumura, H., Kawai, T., and Chao, E. Y. S., 1990, ''Pressure Distribution on Articular Surfaces—Application to Joint Stability Evaluation,'' J. Biomech., **23**, pp. 1013–1020.

[18] Blankevoort, L., Kuiper, J. H., Huiskes, R., and Grootenboer, H. J., 1991, ''Articular Contact in a 3-Dimensional Model of the Knee,'' J. Biomech., **24**, pp. 1019–1031.

[19] Li, G. A., Sakamoto, M., and Chao, E. Y. S., 1997, ''A Comparison of Different Methods in Predicting Static Pressure Distribution in Articulating Joints,'' J. Biomech., **30**, pp. 635–638.

[20] Fregly, B. J., Bei, Y. H., and Sylvester, M. E., 2003, ''Experimental Evaluation of an Elastic Foundation Model to Predict Contact Pressures in Knee Replacements,'' J. Biomech., **36**, pp. 1659–1668.

[21] Kane, T. R., and Levinson, D. A., 1985, *Dynamics: Theory and Applications*, McGraw Hill, New York.

[22] Johnson, F., Scarrow, P., and Waugh, W., 1981, ''Assessments of Loads in the Knee-Joint,'' Med. Biol. Eng. Comput., **19**, pp. 237–243.

[23] Schipplein, O. D., and Andriacchi, T. P., 1991, ''Interaction Between Active and Passive Knee Stabilizers During Levelwalking,'' J. Orthop. Res., **9**, pp. 113–119.

[24] Hurwitz, D. E., Sumner, D. R., Andriacchi, T. P., and Sugar, D. A., 1998, ''Dynamic Knee Loads During Gait Predict Proximal Tibial Bone Distribution,'' J. Biomech., **31**, pp. 423–430.

[25] Lu, T. W., Taylor, S. J. G., O'Connor, J. J., and Walker, P. S., 1997, ''Influence of Muscle Activity on the Forces in the Femur: An in Vivo Study,'' J. Biomech., **30**, pp. 1101–1106.

[26] Taylor, S. J. G., Walker, P. S., Perry, J. S., Cannon, S. R., and Woledge, R., 1998, ''The Forces in the Distal Femur and the Knee During Walking and Other Activities Measured by Telemetry,'' J. Arthroplasty, **13**, pp. 428–437.

[27] Taylor, S. J. G., and Walker, P. S., 2001, ''Forces and Moments Telemetered From Two Distal Femoral Replacements During Various Activities,'' J. Biomech., **34**, pp. 839–848.